NHR-8 regulated P-glycoproteins uncouple xenobiotic stress resistance from longevity in chemosensory *C. elegans* mutants

Gabriel A. Guerrero[1], Matías D. Hartman[1], Klara Schilling[1], Felix A.M.C. Mayr[1], Ryan Lu[4], Bérénice A. Benayoun[4] & Martin S. Denzel[1,2,3]*

[1]Max Planck Institute for Biology of Ageing
Joseph-Stelzmann-Str. 9b
D-50931 Cologne, Germany

[2]CECAD - Cluster of Excellence
University of Cologne
Joseph-Stelzmann-Str. 26
D-50931 Cologne, Germany

[3]Center for Molecular Medicine Cologne (CMMC)
University of Cologne
Robert-Koch-Str. 21
D-50931 Cologne, Germany

[4]Leonard Davis School of Gerontology
University of Southern California
Los Angeles, CA 90089, USA

*correspondence:
mdenzel@age.mpg.de

Abstract

Longevity is often associated with stress resistance, but whether they are causally linked is incompletely understood. Here we investigate chemosensory defective *Caenorhabditis elegans* mutants that are long-lived and stress resistant. We find that mutants in the intraflagellar transport protein gene *osm-3* were significantly protected from tunicamycin-induced ER stress. While *osm-3* lifespan extension is dependent on the key longevity factor DAF-16/FOXO, tunicamycin resistance was not. *osm-3* mutants are protected from bacterial pathogens, which is *pmk-1* p38 MAP kinase dependent while TM resistance was *pmk-1* independent. Inhibition of P-glycoproteins with verapamil suppressed tunicamycin resistance and expression of P-glycoprotein xenobiotic detoxification genes was elevated in *osm-3* mutants. The nuclear hormone receptor *nhr-8* was necessary and sufficient to regulate P-glycoproteins and tunicamycin resistance in a cholesterol-dependent fashion. We thus identify a cell-nonautonomous regulation of xenobiotic detoxification and show that separate pathways are engaged to mediate longevity, pathogen resistance, and xenobiotic detoxification in *osm-3* mutants.

43 **Introduction**

44 Chemosensation is a genetically tractable phenotype in various model organisms. In
45 *C. elegans*, many mutants with defective chemosensation have been identified.
46 Sensory phenotypes are complex in nature and many of the classical chemosensory
47 mutants were originally characterized by their behavioral phenotypes. Odr mutants for
48 example have an abnormal odorant response while Osm (osmotic avoidance
49 abnormal) mutants do not avoid high salt environments (Bargmann, 2006). In mutants
50 like *tax-4* and *odr-1*, mutations in components of neuronal G-protein coupled receptor
51 (GPCR) signaling cause atypical chemosensory behavior (Bargmann, 2006). These
52 mutants are not only characterized by a failure to adequately respond to their
53 environment, but show additional phenotypes linked to various life traits including
54 pathogen resistance, increased lifespan and drug detoxification (Gaglia et al., 2012,
55 Apfeld and Kenyon, 1999, Dent et al., 2000). Many chemosensory mutants are long-
56 lived and this phenotype depends on the DAF-16/FOXO transcription factor that is
57 regulated by the insulin signaling pathway (Apfeld and Kenyon, 1999).

58 Beyond mutations in GPCRs, variants in genes involved in the development of amphid
59 sensory neurons can lead to chemosensory defects. One example are mutations in
60 intraflagellar transport (IFT) proteins that prevent full cilia development of amphid
61 sensory neurons (Inglis et al., 2007). Alterations in the IFT genes *osm-3* and *daf-10*
62 physically disrupt the development of neuronal dendrites that project toward the tip of
63 the nose where they are exposed to the outer environment (Inglis et al., 2007). Thus,
64 IFT mutants are usually characterized by defects in the chemical perception of their
65 environment. Further, developmental defects in lumen formation of the amphid head
66 channel in *daf-6* mutants prevent the direct contact of amphid sensory neurons with
67 the outside (Perens and Shaham, 2005).

68 In wild type (WT) worms, amphid and phasmid sensory neurons can be visualized
69 using the red lipophilic dye DiI, which fluorescently stains them bright red. The dye is
70 passively taken up by sensory neurons when they are fully developed and in contact
71 with the environment. Dye filling defective (Dyf) *C. elegans* are defined by an inability
72 to take up DiI into their sensory neurons (Inglis et al., 2007). The Dyf phenotype arises
73 in *daf-6* animals and also in many IFT mutants. Interestingly, Dyf mutants have unique
74 stress resistance phenotypes that act via different signaling pathways. One such Dyf
75 mutant, *daf-10(m79)*, has a unique resistance to pathogenic bacteria that was
76 proposed to be downstream of sensory input (Gaglia et al., 2012). Further, pairs of
77 amphid head neurons, such as ASH and ASJ that often become disrupted in Dyf
78 mutants help coordinate the innate immune response to bacterial stress after infection
79 (Meisel et al., 2014). Longevity is often associated with activation of physiological
80 stress pathways and has been shown to be regulated by the insulin signaling pathway
81 in Dyf *C. elegans* (Apfeld and Kenyon, 1999).
82 Conserved mechanisms of longevity and stress resistance have additionally been
83 linked to hyposmia in higher model organisms. In *Drosophila melanogaster*, loss of the
84 putative chemoreceptor *Or83b* has been shown to significantly increase lifespan
85 (Libert et al., 2007). Further, mice with ablated olfactory sensory neurons, have a
86 unique metabolic signature that protects them from high-fat diets (Riera et al., 2017).
87 While the olfactory machinery is seemingly more complex in higher organisms,
88 *C. elegans* have unique phenotypes associated with the loss or alteration of their
89 sensory neurons. First, unbiased screens for drug resistance have independently
90 identified the Dyf phenotype as a common feature in drug resistant *C. elegans* (Fujii et
91 al., 2004, Menez et al., 2016, Collins et al., 2008). Selection for resistance to the
92 anthelmintic drug ivermectin was shown to enrich for Dyf mutants in several forward
93 genetic screens (Menez et al., 2016, Page, 2018, Dent et al., 2000). Follo- up work

94 identified P-glycoproteins, a class of ATP binding cassette (ABC) transporters, as the
95 drivers behind ivermectin resistance in Dyf mutants (Ardelli and Prichard, 2013).
96 Second, some chemosensory mutants, such as *daf-10*, show resistance to pathogenic
97 bacteria (Gaglia et al., 2012).
98 Here, we characterize a long-lived Dyf mutant, *osm-3*, that was previously identified in
99 a forward genetic screen for resistance to the potent ER stressor tunicamycin (TM).
100 From this screen, we reported the role of the hexosamine biosynthetic pathway in TM
101 resistance and longevity (Denzel et al., 2014). Our aim was to uncover the mechanism
102 by which Dyf mutants are resistant to TM. We found that the TM resistance of *osm-3*
103 mutants is independent from its longevity and pathogen resistance phenotypes.
104 Further, we showed that P-glycoproteins mediate TM resistance in Dyf animals and
105 we found that the nuclear hormone receptor *nhr-8* mediates *osm-3* drug resistance.
106 The “Green Theory” of ageing proposes that the accumulation of toxic endo- and
107 xenobiotic debris contributes to physiological decline with age (Afschar et al., 2016,
108 Gems and McElwee, 2005). Our work highlights drug resistance as a unique
109 characteristic of Dyf mutants and functionally uncouples it from known stress response
110 pathways that have been implicated in stress resistance and longevity of
111 chemosensory mutants.

112 **Results**

113 **Dye filling defective *C. elegans* mutants are resistant to TM**

114 TM is commonly used to induce endoplasmic reticulum (ER) stress by inhibiting the
115 addition of N-glycans to nascent polypeptides (Parodi, 2000, Heifetz et al., 1979). In
116 *C. elegans*, where the ER machinery is conserved, treatment with TM is toxic and
117 induces the ER unfolded protein response. In fact, on plates containing TM at
118 concentrations above 4 μg/mL, newly hatched larvae die at early developmental
119 stages (Shen et al., 2001). Previously, we had carried out an ethyl methane-sulfonate
120 (EMS) mutagenesis screen to identify TM-resistant and longlived *C. elegans* mutants
121 (Denzel et al., 2014). The largest cohort of classifiable mutants presented dye filling
122 defects (Dyf) (Figure 1A). Dyf mutants are uniquely characterized by their inability to
123 take up the lipophilic red fluorescent dye DiI in their ciliated amphid neurons (Inglis et
124 al., 2007).

125 Among the Dyf mutants from the TM resistance screen, we found new alleles of genes
126 previously linked to ciliary development. The mutant allele we selected for our
127 investigation, *osm-3(dh441)IV* (this allele will be referred to as *osm-3*), carries a
128 premature stop in the eighth exon, which prevents normal cilia development causing
129 the Dyf phenotype (Figure 1A, Figure 1-figure supplement 1A). *osm-3* is a member of
130 the kinesin family involved in axonal transport and development and mutants are
131 known to show a Dyf phenotype (Inglis et al., 2007). While WT worms fail to develop
132 on TM at concentrations above 4 μg/mL, *osm-3* mutants fully develop at
133 concentrations at least up to 10 μg/mL TM (Figure 1B). Loss of OSM-3, as well as
134 other Dyf mutations, promote longevity in *C. elegans* (Apfeld and Kenyon, 1999).
135 Demographic lifespan analysis of *osm-3* indeed confirmed extended lifespan in our
136 point mutant (Figure 1C and Supplementary Table 1). *osm-3* mutants, and Dyf mutants

137 in general, have never been described as TM resistant especially at concentrations as
138 high as 10 μg/mL.
139 To further explore whether the Dyf phenotype is linked to TM resistance we tested
140 other Dyf mutants that were previously described as long-lived in the literature (Apfeld
141 and Kenyon, 1999). To our surprise, all Dyf mutants that we tested proved to be
142 significantly TM resistant at the WT lethal dose of 10 μg/mL TM (Figure 1D,F). In
143 contrast, the long-lived chemosensory mutants *odr-1(n1936)X* and *odr-3(n2150)V* that
144 display no Dyf phenotype were only slightly TM resistant (Figure 1E,F, Figure 1-figure
145 supplement 1B-J). Our data thus suggest phenotypic differences regarding TM
146 resistance among the larger class of chemosensory defective mutants.
147
148 **ER stress response is blunted in *osm-3* mutants**
149 TM treatment activates the ER unfolded protein response (UPR^{ER}); we thus
150 characterized the overall transcriptional response of *osm-3* mutants upon TM
151 treatment. We performed transcriptomic analyses on *osm-3* and WT worms after
152 6 hours of TM treatment. Notably, the gene ontology (GO) terms related to ER stress
153 and ER protein folding showed significant upregulation in WT animals but not in *osm-*
154 *3* mutants (Figure 2A). qPCR analysis of UPR target genes further confirmed that there
155 was no UPR^{ER} induction in the TM-treated *osm-3* mutants compared to the WT
156 (Figure 2-figure supplement 1). A hallmark of UPR^{ER} induction in *C. elegans* is the
157 upregulation of the molecular chaperone HSP-4/BiP (Shen et al., 2001). Upon TM
158 treatment of *osm-3* mutants carrying an *hsp-4*::GFP reporter construct, there was no
159 significant increase in the GFP signal compared to the untreated control, while in the
160 WT the GFP levels were significantly increased (Figure 2B,C). This observation
161 corroborates the results from the transcriptome analysis.

162 One potential explanation for a suppressed UPR^{ER} response in *osm-3* mutants might
163 be a general defect in the stress signaling pathway. To address this possibility, we
164 sought to activate the UPR by alternate means. The ER membrane protein SEL-
165 1/HRD3 is a cofactor of the HRD1 ubiquitin ligase complex involved in ER-associated
166 degradation (ERAD)(Hampton et al., 1996). Using *sel-1* RNAi to inhibit ERAD, we
167 observed a robust activation of the *hsp-4*::GFP reporter, suggesting a functional
168 UPR^{ER} response upon ER stress (Figure 2D,E). We further used DTT treatment to
169 induce ER stress and found normal levels of *hsp-4*::GFP induction and *xbp-1* splicing
170 (Figure 2F) in *osm-3* mutants. Together, these observations rule out that the reduced
171 response to TM observed in *osm-3* mutants was due to a defect in UPR signaling.
172

173 **TM resistance in *osm-3* mutants is independent from *daf-16* or the PMK-1/p38**
174 **MAPK pathway**

175 The lifespan extension observed in chemosensory defective *C. elegans* as well as in
176 *Drosophila* has been shown to be at least partially insulin signaling dependent (Apfeld
177 and Kenyon, 1999, Libert et al., 2007). Therefore, we performed a demographic
178 lifespan analysis to determine the role of the insulin signaling pathway in the lifespan
179 extension of *osm-3* mutants. Indeed, the *osm-3* lifespan extension was fully *daf-16*
180 dependent, as the lifespan of the *osm-3; daf-16* double mutants was identical to the
181 *daf-16* lifespan (Figure 3A, Supplementary Table 1). To our surprise, the *osm-3; daf-*
182 *16* double mutant was resistant to TM while *daf-16* single mutants do not develop at
183 10 μg/mL TM (Figure 3B). A previous study by Henis-Korenblit et al. had shown
184 elevated *hsp-4*::GFP levels during *daf-16* knockdown in a *daf-2* mutant (Henis-
185 Korenblit et al., 2010). We therefore asked whether the knockdown of *daf-16* would
186 sensitize *osm-3* mutants to TM. Interestingly, knock-down of *daf-16* by RNAi did not
187 rescue the *hsp-4*::GFP response after TM treatment (Figure 3-figure supplement 1).

188 Given the links between the insulin signaling pathway and the ER stress signaling
189 (Henis-Korenblit et al., 2010, Kyriakakis et al., 2017, Matai et al., 2019, Labbadia and
190 Morimoto, 2014), we were further surprised to find that *daf-2* mutants failed to develop
191 on 10 μg/mL TM while *osm-3* mutants fully developed (Figure 3C). Together, this
192 evidence suggests that the *osm-3* lifespan extension and TM drug resistance are
193 uncoupled and instead appear to act via independent or parallel pathways.
194 In *C. elegans, Pseudomonas aeruginosa* PA14 is a pathogen that is often used to
195 study innate immunity. Of note, UPR^{ER} targets have been implicated in the innate
196 immune response of *C. elegans* during PA14 infection (Richardson et al., 2010,
197 Haskins et al., 2008). As the ER plays a role in innate immunity and as TM disrupts ER
198 function, we speculated that *osm-3* mutants would be more robust on PA14 than WT.
199 Indeed, *osm-3* mutants were more resistant to PA14 than WT, however this increased
200 pathogen resistance was suppressed by loss of the PMK-1 p38 mitogen-activated
201 protein kinase (MAPK) pathway (Figure 3D). With this in mind, we tested whether *pmk-*
202 *1* mutation could suppress the *osm-3* TM resistance. The *osm-3; pmk-1* double mutant
203 was fully resistant to TM, while the *pmk-1* single was sensitive (Figure 3E). Taken
204 together, insulin signaling and the MAPK pathway, two major stress response
205 pathways in *C. elegans* that have links to ER protein quality control, are not required
206 for TM resistance in *osm-3* mutants.
207

208 **P glycoprotein inhibition suppresses *osm-3* TM resistance**

209 Given the lack of ER stress in TM-treated *osm-3* mutants along with the genetic
210 separation of TM resistance from insulin or MAPK signaling, we hypothesized that TM
211 might be cleared from worm tissues through xenobiotic detoxification. To test this, we
212 used verapamil (VPL) to inhibit P-glycoproteins (PGPs) that secrete toxins. PGPs are
213 a conserved family of ATP binding cassette (ABC) transporters found on the cell

214 membrane (Sangster, 1994) and *C. elegans* have 15 PGP genes. VPL has been used
215 to specifically inhibit PGP activity, re-sensitizing worms to the antihelmintic compound
216 ivermectin (Menez et al., 2016). Indeed, 1 nM VPL significantly suppressed
217 development of *osm-3 C. elegans* in the presence of TM, while having no effect on
218 controls without TM (Figure 4A).
219 Dyf *C. elegans* mutants have been independently identified in drug resistance screens
220 (Fujii et al., 2004, Menez et al., 2016, Dent et al., 2000). Consistent with these findings,
221 we observed that *osm-3* mutants were resistant to 200 nM methyviologen dichloride
222 (paraquat), as they fully develop at a concentration that is toxic to WT *C. elegans*
223 (Figure 4B). Similarly, *osm-3* mutants fully developed to adults in the presence of
224 6 μg/mL ivermectin that is lethal to WT animals (Figure 4C). In contrast, *osm-3* mutants
225 showed no difference to WT animals in heat stress assays or in the presence of
226 hydrogen peroxide (H_2O_2) suggesting that *osm-3* mutants are not resistant to non-
227 xenobiotic stressors (Figure 4-figure supplement 1A,B). While paraquat and hydrogen
228 peroxide are both oxidative stressors, paraquat acts indirectly via the mitochondria
229 (Castello et al., 2007) while hydrogen peroxide is a primary cause for oxidative
230 damage. Thus, we view paraquat as a xenobiotic stressor. Given the involvement of
231 PGP-dependent xenobiotic detoxification in TM resistance of *osm-3* mutants , we
232 wondered about its role in the longevity of *osm-3* mutants. Notably, VPL did not shorten
233 *osm-3* lifespan (Figure 4D). Moreover, VPL did not affect WT lifespan (Figure 4D and
234 Supplementary Table 1) and had no visible effect on WT development (Figure 4-figure
235 supplement 1C). Together, these data support the conclusion that the xenobiotic stress
236 resistance and longevity phenotypes of *osm-3* mutants are mediated by independent
237 pathways.
238
239 **NHR-8 signaling regulates xenobiotic detoxification response through PGPs**

240 VPL treatment suggested a role for PGPs in the TM resistance of *osm-3* mutants.
241 Using quantitative PCR we found a significant upregulation of *pgp-3*, *pgp-5*, *pgp-8*,
242 *pgp-11*, and *pgp-13* in *osm-3* mutants (Figure 5A). The nuclear hormone receptor
243 NHR-8 has been linked to xenobiotic detoxification and PGP regulation in *C. elegans*
244 (Menez et al., 2019, Lindblom et al., 2001). Indeed, we found that the upregulation of
245 PGP expression in *osm-3* mutants was suppressed in the *osm-3; nhr-8* double mutant
246 (Figure 5A). This led us to ask whether *osm-3* TM resistance was dependent on NHR-
247 8 signaling. Indeed, the *osm-3; nhr-8(hd117)IV* double mutant was not resistant to TM
248 while the *osm-3* mutant fully developed (Figure 5B), suggesting that NHR-8 is
249 necessary for *osm-3* TM resistance. We next asked if NHR-8 was sufficient for TM
250 resistance using a transgenic overexpressor (Magner et al., 2013). Of note, we found
251 a significant upregulation of *pgp-8* in *nhr-8* transgenic animals (Figure 5C). In a
252 developmental TM dose response assay, we found that overexpression of *nhr-8* in WT
253 worms results in significant TM resistance (Figure 5D). Characterization of UPR^{ER}
254 signaling using the *hsp-4::*GFP reporter showed that *pgp-8* RNAi sensitizes *osm-3*
255 mutants to TM. This experiment was done at 20 μg/mL TM to induce a mild ER stress
256 in *osm-3* mutants. Together, these data suggest that TM stress resistance in *osm-3*
257 mutants is due to effective xenobiotic detoxification that is mediated by NHR-8 and
258 PGPs. Consistent with previous studies (Magner et al., 2013), we found that *nhr-8*
259 mutation shortened lifespan and that it, likewise, shortened *osm-3* survival (Figure 5-
260 figure supplement 1).
261

262 **Sterol signals modulate TM resistance**

263 We next wanted to further understand the systemic signals that control xenobiotic
264 detoxification of TM. The NHR-8 ligand remains unknown, but is likely a sterol molecule
265 derived from cholesterol metabolism (Magner et al., 2013). We thus tested the role of

266 cholesterol in TM resistance and found that omitting cholesterol from the culture plate
267 for one generation leads to TM hypersensitivity in both WT and *osm-3* animals
268 (Figure 6A). Developmental cholesterol dose response assays in the presence of TM
269 confirmed that WT TM resistance is cholesterol dependent (Figure 6B). In *nhr-8* and
270 *osm-3; nhr-8* double mutants, however, cholesterol treatment failed to protect from TM
271 developmental toxicity. This demonstrates a key role of NHR-8 in mediating TM
272 resistance downstream from sterol signals. To corroborate a role of cholesterol derived
273 signals in TM resistance, we used the *hsp-4*::GFP reporter and found that high
274 cholesterol significantly reduced TM-induced ER stress (Figure 6C). Consistent with
275 this, *pgp-8* was upregulated by high cholesterol treatment (Figure 6D). These
276 observations suggest cell-nonautonomous regulation of xenobiotic detoxification of TM
277 by cholesterol-derived ligands that enhance PGP expression via NHR-8.

278 **Discussion**

279 In this study, we found that *osm-3* mutants as well as other Dyf mutants are resistant
280 to the ER toxin TM. Instead of an activated stress signaling status that might explain
281 the TM resistance, *osm-3* Dyf mutants show no UPR^{ER} induction upon TM treatment.
282 Consistent with previous findings (Apfeld and Kenyon, 1999) the lifespan extension of
283 *osm-3* was *daf-16* dependent. Despite the established link between the insulin
284 signaling pathway and stress resistance, the TM resistance in *osm-3* mutants was not
285 insulin signaling dependent. Further, while *osm-3* mutants were pathogen resistant,
286 this resistance was fully dependent on the PMK-1/p38 MAPK pathway. We were
287 surprised that neither of the two pathways weakened the TM resistance phenotype.
288 Dyf *C. elegans* drug resistance is not specific to TM, as we also observed resistance
289 to paraquat and ivermectin. While paraquat and ivermectin resistance have been
290 previously reported in Dyf mutants (Dent et al., 2000, Fujii et al., 2004, Menez et al.,
291 2016), no studies have demonstrated similar resistance mechanisms in Dyf *C. elegans*
292 mutants to TM. Our findings show that this resistance is due to increased PGP
293 expression in Dyf worms. Importantly, we demonstrate regulation of PGPs by
294 cholesterol and the nuclear hormone receptor NHR-8. Broad inhibition of PGPs using
295 verapamil or loss of *nhr-8* significantly re-sensitized *osm-3* mutants to TM.
296 Consistently, NHR-8 overexpression or high cholesterol treatment resulted in TM
297 resistance in WT animals.

298 Given that improved protein homeostasis is one of the cellular hallmarks of longevity
299 (Lopez-Otin et al., 2013), we presumed that selection for TM resistance would serve
300 as a proxy phenotype for longevity given that TM specifically targets ER protein folding.
301 More specifically, we expected that high fidelity ER protein quality control would be the
302 driver of longevity in these mutants. Previous findings describing increased
303 hexosamine biosynthetic pathway flux (Denzel et al., 2014) or constitutive XBP-1

304 activation (Taylor and Dillin, 2013) have linked protein homeostasis to longevity and
305 stress resistance (Denzel and Antebi, 2015); therefore the connection between TM
306 resistance and longevity seemed apparent. Given that Dyf mutants are resistant to
307 pathogenic bacteria through enhanced ER homeostasis, we also speculated that TM
308 resistance might serve as a proxy phenotype for pathogen resistance. On the contrary,
309 we found that xenobiotic detoxification via PGPs is sufficient for TM resistance but not
310 longevity in *osm-3* mutants. *pmk-1* and *daf-16* were required for pathogen resistance
311 and longevity, respectively. Whether the longevity phenotype of *osm-3* mutants would
312 be suppressed by *nhr-8* disruption is difficult to assess as *nhr-8* mutants themselves
313 show decreased survival (Magner et al., 2013).
314 Adding another dimension to the cell-nonautonomous regulation of innate immunity
315 (Aballay, 2013), we propose that the nervous system regulates systemic xenobiotic
316 detoxification *C. elegans*, likely through a sterol ligand. Our data suggest that mutants
317 with defective amphid neurons have increased PGP expression. Several PGPs have
318 been shown to be expressed in non-neuronal tissue (Lincke et al., 1993, Sheps et al.,
319 2004). Moreover, we found that PGP expression is regulated by *nhr-8*, which has also
320 been shown to be expressed in the intestine of *C. elegans* (Magner et al., 2013).
321 Combining this previous information with our finding that Dyf mutants are resistant to
322 several uniquely toxic drugs, we conclude that neuronal signaling controls drug
323 resistance through nuclear hormone signaling. Given our observation that
324 supplementation with cholesterol is itself sufficient for TM resistance in WT worms one
325 might further investigate the link between neuronal states and the specific cholesterol-
326 derived signal that drives these drug resistance phenotypes.
327 PGPs are likely regulated in *C. elegans* to help them combat toxins found in their
328 natural habitat. Toxic metabolites are undoubtedly common in the soil where
329 *C. elegans* are found. The drugs used in our study, ivermectin (a derivative of

330 avermectin) (Burg et al., 1979) and TM, were first discovered as antibiotics that are
331 produced by soil bacteria (Takatsuki et al., 1971). Because *C. elegans* have no
332 adaptive immune response, having PGPs as part of their innate immune system allows
333 them to clear toxic molecules they may encounter in the wild. While Dyf mutants do
334 not occur in the wild, our data nonetheless demonstrate a link environmental sensing
335 and drug resistance.
336 In humans, PGPs have been implicated in drug resistant malignancies (Lehne, 2000).
337 Using *C. elegans* as a tool to study the cross talk between tissues, one might be able
338 to better understand how extracellular signaling drives ABC transporter expression in
339 chemotherapy resistant cancer. Further studies in cell culture might also further
340 characterize TM, as well as other toxic metabolites, as substrates for *C. elegans* PGPs.

341 **Materials and Methods**

Key Resources Table				
Reagent type (species) or resource	**Designation**	**Source or reference**	**Identifiers**	**Additional information**
strain, strain background (*E. coli*)	HT115 [*L4440::sel-1*]	Source Bioscience	CELE_F45D3.5	Ahringer RNAi library
strain, strain background (*E. coli*)	HT115 [*L4440::daf-16*]	Source Bioscience	CELE_R13H8.1	Ahringer RNAi library
strain, strain background (*E. coli*)	HT115 [*L4440::pgp-8*]	Source Bioscience	CELE_T21E8.3	Ahringer RNAi library
genetic reagent (*C. elegans*)	*osm-3(dh441)IV*	other	AA1962	available from A. Antebi or M.S. Denzel
genetic reagent (*C. elegans*)	*daf-16(mu86)I*	CGC	CF1038	
genetic reagent (*C. elegans*)	*pmk-1(km25)IV*	CGC	KU25	
genetic reagent (*C. elegans*)	*osm-3(dh441)IV; nhr-8(hd117)IV*	this paper	MSD420	available from M.S. Denzel
genetic reagent (*C. elegans*)	*osm-3(dh441)IV; daf-16(mu86)I*	this paper	MSD422	available from M.S. Denzel

genetic reagent (*C. elegans*)	*osm-3(dh441)IV; pmk-1(km25)IV*	this paper	MSD423	available from M.S. Denzel
genetic reagent (*C. elegans*)	*daf-6(e1377)X*	CGC	CB1377	
genetic reagent (*C. elegans*)	*odr-1(n1936)X*	CGC	CX2065	
genetic reagent (*C. elegans*)	*odr-3(n2150)V*	CGC	CX2205	
genetic reagent (*C. elegans*)	*osm-6(p811)V*	CGC	PR811	
genetic reagent (*C. elegans*)	*tax-4(p678)III*	CGC	PR678	
genetic reagent (*C. elegans*)	*nhr-8(hd117)IV*	other	AA968	available from A. Antebi or M.S. Denzel
genetic reagent (*C. elegans*)	*N2; dhEx451(nhr-8::gfp; coel::RFP)*	CGC	AA1027	
genetic reagent (*C. elegans*)	*osm-3(dh441)IV; zcIs4 [hsp-4::GFP]V*	other	AA2774	available from A. Antebi or M.S. Denzel
genetic reagent (*C. elegans*)	*zcIs4[hsp-4::GFP]V*	CGC	SJ4005	
genetic reagent (*C. elegans*)	*che-11(e1810)V*	CGC	CB3330	

genetic reagent (*C. elegans*)	*daf-10(e1387)IV*	CGC	CB1387	
genetic reagent (*C. elegans*)	*osm-1(p808)X*	CGC	PR808	
genetic reagent (*C. elegans*)	*dyf-1(mn335)I*	CGC	SP1205	
genetic reagent (*C. elegans*)	*che-2(e1033)X*	CGC	CB1033	
genetic reagent (*C. elegans*)	*osm-5(p813)X*	CGC	PR813	
commercial assay or kit	Direct-zol RNA Microprep	Zymo Research	R2060	
commercial assay or kit	SMARTer Stranded RNA-Seq HT Kit	Takara	634838	
commercial assay or kit	Ribo-zero Gold kit	Illumina	MRZG12324	
chemical compound, drug	Tunicamycin	Calbiochem	CAS 11089-65-9	
chemical compound, drug	Dithiothreitol	Sigma Aldrich	CAS 3483-12-3	
chemical compound, drug	Methyl viologen dichloride hydrate	Sigma Aldrich	CAS 75365-73-0	Paraquat
chemical compound, drug	Ivermectin	Sigma Aldrich	CAS 70288-86-7	
chemical compound, drug	Verapamil hydrochloride	Sigma Aldrich	CAS 152-11-4	

chemical compound , drug	Cholesterol	Sigma Aldrich	CAS 57-88-5	
chemical compound , drug	1,1′-Dioctadecyl-3,3,3′,3′-tetramethylindocarbocyanine perchlorate	Sigma Aldrich	CAS 41085-99-8	DiI
software, algorithm	R statistical software	cran.r-project.org	DESeq2 1.16.1	PMID: 25516281
other	Reference Genome	ENSEMBL	WBCel235	

342

343 **Worm maintenance**

344 *C. elegans* nematodes were cultured using standard husbandry methods at 20°C on
345 nematode growth media (NGM) agar plates seeded with *E. coli* strain OP50 unless
346 otherwise stated (Brenner, 1974).

347 **Dye filling assay in *C. elegans***

348 The dye filling assay was performed on a synchronized population of day 1 adults. 40-
349 60 adult worms were placed in M9 containing 10 μg/mL DiI. They were left at room
350 temperature for two hours in the staining medium, then transferred to NGM plates
351 seeded with *E. coli* OP50. The worms were then allowed to crawl on the food for one
352 hour to allow for the dye to be cleared from the gut. The worms were scored for dye
353 filling using a Leica SPX-8 confocal microscope or a Leica fluorescent stereo-
354 microscope. Images were taken using the confocal microscope.

355 **Drug resistance assays**

356 NGM plates containing either TM, paraquat or ivermectin were used in developmental
357 assays to test for resistance. To this end, we performed a 4h egg lay on NGM plates
358 at room temperature then transferred the eggs to control and drug containing plates
359 and recorded the number of eggs per plate. After incubation for four days at 20°C,
360 plates were scored by counting the total number of L4 larvae or adults on each plate.

361 Paraquat plates were prepared by adding 1M methyl viologen dichloride (paraquat)
362 directly onto seeded NGM plates for a final concentration of 200 μM and allowed to dry
363 immediately before use. Ivermectin plates were prepared by adding ivermectin directly
364 to the NGM medium at a final concentration of 6 μg/mL before pouring the plates.
365 Modified NGM plates containing no cholesterol were made by using standard NGM
366 without the addition of cholesterol. NGM agar plates containing 5, 25 or 50 μg/mL
367 Cholesterol were used for development when specifically stated. These modified NGM
368 plates were then supplemented with drugs as described above. All of the drug
369 development assays were performed using *E. coli* OP50 or *E. coli* HT115 bacteria. For
370 the developmental TM dose response assay with the *nhr-8* transgenic dhEx451 strain
371 in Figure 5D, the transgene transmission rate was reported on a separate plate for
372 each condition that was then used for the calculation of the successfully developed
373 proportion of animals.

374 **ER stress quantification**

375 Synchronized day 1 adults were transferred to control and TM containing NGM plates
376 seeded with OP50. After 6 hours of stress induction *hsp-4*::GFP levels were measured
377 by large particle flow cytometry in both the WT and *osm-3(dh441)IV* background using
378 the Union Biometrica Biosorter and imaged using a Leica fluorescent stereo-
379 microscope. For RNAi experiments, animals were raised on control and *daf-16*, *sel-1*
380 or *pgp-8* RNAi. Synchronized day 1 adults were transferred to vehicle or TM containing
381 plates seeded with control or experimental RNAi. After 6 hours of stress, GFP levels
382 were measured using the Biosorter. GFP values were normalized to time of flight. At
383 least 100 animals were analyzed per condition. For RNA isolation, day 1 adults were
384 treated with 10 mM DTT in S Basal buffer containing *E. coli* OP50 for 2 hours and then
385 snap frozen.

386 **Quantitative PCR**

387 For ER stress induction day 1 adults were washed from their plates and transferred to
388 either control or TM containing plates, where they were incubated for 6h. The animals
389 were then washed off using M9 and snap frozen in trizol. Unstressed synchronized
390 animals were collected at day 1 of adult hood for RNA extraction. RNA was prepared
391 using Zymo Research Direct-zol RNA Microprep kit. SYBR green was used to perform
392 quantitative PCR (RT-qPCR). See Supplementary Table 2 for list of qPCR primers
393 used in this study. Primer efficiency was tested and was always above 90%.

394 **Lifespan analysis**

395 Adult lifespan analysis was performed at 20°C on mutant and WT *C. elegans*. The
396 animals were synchronized in a four-hour egg lay. Animals were scored as dead or
397 alive every second day until the end of the experiment. Animals were transferred every
398 day for the first seven days. Statistical analysis on the Kaplan-Meier survival curves
399 was performed using Microsoft Excel. See Supplementary Table 1 for lifespan
400 statistics. Each survival experiment was performed at least twice.

401 **Hydrogen peroxide survival assay**

402 1M hydrogen peroxide (H_2O_2) was added to unseeded NGM plates to a final
403 concentration of 1 μM and allowed to dry for several minutes. Synchronized day one
404 adults were then transferred onto the plates and incubated at 25°C. The animals were
405 then scored every 2 hours for survival. 20 to 50 animals were used in each
406 experimental condition.

407 **Pathogenic bacteria survival assay**

408 The *Pseudomonas aeruginosa* strain PA14 was grown in LB media and seeded onto
409 high peptone NGM plates and incubated for 12 hours at 37°C immediately before the
410 start of the experiment. Day one animals were first transferred to unseeded NGM

411 plates to crawl around the plate and remove any excess *E. coli* OP50 off of their bodies.
412 They were then transferred to the PA14 containing plates and incubated at 25°C. The
413 animals were scored every 12 hours until all animals were dead. At least 75 animals
414 were used in each experimental condition.

415 **Heat stress survival assay**

416 Day 1 synchronized *C. elegans* were transferred to fresh NGM plates seeded with *E.*
417 *coli* OP50. These plates were transferred to a 35°C incubator, where they were evenly
418 distributed throughout the incubator to ensure even heat exposure. The plates were
419 scored for live worms every 2 hours until all of the worms were dead. 20 to 50 animals
420 were used in each experimental condition.

421 **Sample collection and RNA purification for sequencing**

422 For RNA sequencing we used day one adults that were hatched within one hour. To
423 achieve this synchronization, we washed all adults and larvae of plates with M9 and
424 allowed the eggs on hatch for one hour. The freshly hatched L1 larvae were then
425 washed off and transferred to fresh plates seeded with OP50 and incubated at 20°C
426 until they developed to adults. At day one of adulthood, animals were washed from
427 their plates and transferred to either control or TM containing plates, where they were
428 incubated for 6 hours. The animals were then washed off using M9 and snap frozen in
429 trizol. All biological replicates were collected and prepared using a snaking collection
430 method to reduce batch effects. Total RNA was purified using Zymo Research Direct-
431 zol RNA Microprep kit.

432 **RNA-seq library preparation**

433 RNA quality was assessed using Agilent's Bioanalyzer platform, and samples with RIN
434 > 9 were used for library construction. 2.5 µg of total RNA was subjected to ribosomal
435 RNA (rRNA) depletion using the Illumina's Ribo-zero Gold kit (Illumina), according to

436 the manufacturer's protocol. Strand specific RNA-seq libraries were then constructed
437 using the SMARTer Stranded RNA-Seq HT Kit (Clontech #634839), according to the
438 manufacturer's protocol. Based on rRNA-depleted input amount, 15 cycles of
439 amplification were performed to generate RNA-seq libraries. Paired-end 150 bp reads
440 were sent for sequencing on the Illumina HiSeq-Xten platform at the Novogene
441 Corporation (USA). The resulting data was then analyzed with a standardized RNA-
442 seq data analysis pipeline (described below).

443 **RNA-seq analysis pipeline**

444 cDNA sequences of worm genes were obtained through ENSEMBL Biomart for the
445 WBCel235 build of the *C. elegans* genome (Ensemble release v94; accessed 2018-
446 12-03). Trimmed reads were mapped to this reference using kallisto 0.43.0-1 and the
447 –fr-stranded option (Bray et al., 2016). All subsequent analyses were performed in the
448 R statistical software (https://cran.r-project.org/). Read counts were imported into R,
449 and summarized at the gene level. Differential gene expression was estimated using
450 the 'DESeq2' R package (DESeq2 1.16.1) (Love et al., 2014). David analysis (version
451 6.8) was performed to identify significantly enriched gene ontology terms.

452 **Developmental verapamil (VPL) resistance assay and lifespan analysis**

453 Plates containing 10 μg/mL TM were supplemented with 1 nM VPL by adding VPL
454 solved in DMSO onto the plates. Plates were allowed to dry for 6h before eggs were
455 transferred to them to determine developmental resistance to TM. Plates were then
456 scored after 4 days to determine the relative number of L4 larvae or adults. Lifespan
457 assays were performed as above, however the animals were transferred to fresh VPL
458 containing plates every second day for the whole lifespan assay. 20 to 50 animals were
459 used in each experimental condition.

460

461 **Data availability**

462 Raw sequencing data were deposited to the NCBI Gene Expression Omnibus (GEO)
463 under the accession number GSE144675.

464 **Acknowledgements**

465 We thank all M.S.D. laboratory members for lively and helpful discussions. We thank
466 Adam Antebi for valuable comments and for *C. elegans* strains. We thank Seung-Jae
467 Lee for valuable comments on the manuscript. We thank the Caenorhabditis Genetics
468 Center (CGC) for strains. We thank the members of the bioinformatics core facility and
469 the FACS and imaging core facility at MPI AGE. B.A.B is supported by a seed grant
470 from the NAVIGAGE foundation, and a generous gift from the Hanson-Thorell Family.
471 M.S.D. was supported by ERC-StG 640254, by the Deutsche
472 Forschungsgemeinschaft (DFG, German Research Foundation) - Projektnummer
473 73111208 - SFB 829, and by the Max Planck Society.

474 **Competing interests**

475 The authors declare no competing interests.

References

ABALLAY, A. 2013. Role of the nervous system in the control of proteostasis during innate immune activation: insights from C. elegans. *PLoS Pathog,* 9**,** e1003433.

AFSCHAR, S., TOIVONEN, J. M., HOFFMANN, J. M., TAIN, L. S., WIESER, D., FINLAYSON, A. J., DRIEGE, Y., ALIC, N., EMRAN, S., STINN, J., FROEHLICH, J., PIPER, M. D. & PARTRIDGE, L. 2016. Nuclear hormone receptor DHR96 mediates the resistance to xenobiotics but not the increased lifespan of insulin-mutant Drosophila. *Proc Natl Acad Sci U S A,* 113**,** 1321-6.

APFELD, J. & KENYON, C. 1999. Regulation of lifespan by sensory perception in Caenorhabditis elegans. *Nature,* 402**,** 804-9.

ARDELLI, B. F. & PRICHARD, R. K. 2013. Inhibition of P-glycoprotein enhances sensitivity of Caenorhabditis elegans to ivermectin. *Vet Parasitol,* 191**,** 264-75.

BARGMANN, C. I. 2006. Chemosensation in C. elegans. *WormBook***,** 1-29.

BRAY, N. L., PIMENTEL, H., MELSTED, P. & PACHTER, L. 2016. Near-optimal probabilistic RNA-seq quantification. *Nat Biotechnol,* 34**,** 525-7.

BRENNER, S. 1974. The genetics of Caenorhabditis elegans. *Genetics,* 77**,** 71-94.

BURG, R. W., MILLER, B. M., BAKER, E. E., BIRNBAUM, J., CURRIE, S. A., HARTMAN, R., KONG, Y. L., MONAGHAN, R. L., OLSON, G., PUTTER, I., TUNAC, J. B., WALLICK, H., STAPLEY, E. O., OIWA, R. & OMURA, S. 1979. Avermectins, new family of potent anthelmintic agents: producing organism and fermentation. *Antimicrob Agents Chemother,* 15**,** 361-7.

CASTELLO, P. R., DRECHSEL, D. A. & PATEL, M. 2007. Mitochondria are a major source of paraquat-induced reactive oxygen species production in the brain. *J Biol Chem,* 282**,** 14186-93.

COLLINS, J. J., EVASON, K., PICKETT, C. L., SCHNEIDER, D. L. & KORNFELD, K. 2008. The anticonvulsant ethosuximide disrupts sensory function to extend C. elegans lifespan. *PLoS Genet,* 4**,** e1000230.

DENT, J. A., SMITH, M. M., VASSILATIS, D. K. & AVERY, L. 2000. The genetics of ivermectin resistance in Caenorhabditis elegans. *Proc Natl Acad Sci U S A,* 97**,** 2674-9.

DENZEL, M. S. & ANTEBI, A. 2015. Hexosamine pathway and (ER) protein quality control. *Curr Opin Cell Biol,* 33**,** 14-8.

DENZEL, M. S., STORM, N. J., GUTSCHMIDT, A., BADDI, R., HINZE, Y., JAROSCH, E., SOMMER, T., HOPPE, T. & ANTEBI, A. 2014. Hexosamine pathway metabolites enhance protein quality control and prolong life. *Cell,* 156**,** 1167-1178.

FUJII, M., MATSUMOTO, Y., TANAKA, N., MIKI, K., SUZUKI, T., ISHII, N. & AYUSAWA, D. 2004. Mutations in chemosensory cilia cause resistance to paraquat in nematode Caenorhabditis elegans. *J Biol Chem,* 279**,** 20277-82.

GAGLIA, M. M., JEONG, D. E., RYU, E. A., LEE, D., KENYON, C. & LEE, S. J. 2012. Genes that act downstream of sensory neurons to influence longevity, dauer formation, and pathogen responses in Caenorhabditis elegans. *PLoS Genet,* 8**,** e1003133.

GEMS, D. & MCELWEE, J. J. 2005. Broad spectrum detoxification: the major longevity assurance process regulated by insulin/IGF-1 signaling? *Mech Ageing Dev,* 126**,** 381-7.

HAMPTON, R. Y., GARDNER, R. G. & RINE, J. 1996. Role of 26S proteasome and HRD genes in the degradation of 3-hydroxy-3-methylglutaryl-CoA reductase, an integral endoplasmic reticulum membrane protein. *Mol Biol Cell,* 7**,** 2029-44.

HASKINS, K. A., RUSSELL, J. F., GADDIS, N., DRESSMAN, H. K. & ABALLAY, A. 2008. Unfolded protein response genes regulated by CED-1 are required for Caenorhabditis elegans innate immunity. *Dev Cell,* 15**,** 87-97.

HEIFETZ, A., KEENAN, R. W. & ELBEIN, A. D. 1979. Mechanism of action of tunicamycin on the UDP-GlcNAc:dolichyl-phosphate Glc-NAc-1-phosphate transferase. *Biochemistry,* 18**,** 2186-92.

HENIS-KORENBLIT, S., ZHANG, P., HANSEN, M., MCCORMICK, M., LEE, S. J., CARY, M. & KENYON, C. 2010. Insulin/IGF-1 signaling mutants reprogram ER stress response regulators to promote longevity. *Proc Natl Acad Sci U S A,* 107**,** 9730-5.

INGLIS, P. N., OU, G., LEROUX, M. R. & SCHOLEY, J. M. 2007. The sensory cilia of Caenorhabditis elegans. *WormBook*, 1-22.
KYRIAKAKIS, E., CHARMPILAS, N. & TAVERNARAKIS, N. 2017. Differential adiponectin signalling couples ER stress with lipid metabolism to modulate ageing in C. elegans. *Sci Rep,* 7, 5115.
LABBADIA, J. & MORIMOTO, R. I. 2014. Proteostasis and longevity: when does aging really begin? *F1000Prime Rep,* 6, 7.
LEHNE, G. 2000. P-glycoprotein as a drug target in the treatment of multidrug resistant cancer. *Curr Drug Targets,* 1, 85-99.
LIBERT, S., ZWIENER, J., CHU, X., VANVOORHIES, W., ROMAN, G. & PLETCHER, S. D. 2007. Regulation of Drosophila life span by olfaction and food-derived odors. *Science,* 315, 1133-7.
LINCKE, C. R., BROEKS, A., THE, I., PLASTERK, R. H. & BORST, P. 1993. The expression of two P-glycoprotein (pgp) genes in transgenic Caenorhabditis elegans is confined to intestinal cells. *EMBO J,* 12, 1615-20.
LINDBLOM, T. H., PIERCE, G. J. & SLUDER, A. E. 2001. A C. elegans orphan nuclear receptor contributes to xenobiotic resistance. *Curr Biol,* 11, 864-8.
LOPEZ-OTIN, C., BLASCO, M. A., PARTRIDGE, L., SERRANO, M. & KROEMER, G. 2013. The hallmarks of aging. *Cell,* 153, 1194-217.
LOVE, M. I., HUBER, W. & ANDERS, S. 2014. Moderated estimation of fold change and dispersion for RNA-seq data with DESeq2. *Genome Biol,* 15, 550.
MAGNER, D. B., WOLLAM, J., SHEN, Y., HOPPE, C., LI, D., LATZA, C., ROTTIERS, V., HUTTER, H. & ANTEBI, A. 2013. The NHR-8 nuclear receptor regulates cholesterol and bile acid homeostasis in C. elegans. *Cell Metab,* 18, 212-24.
MATAI, L., SARKAR, G. C., CHAMOLI, M., MALIK, Y., KUMAR, S. S., RAUTELA, U., JANA, N. R., CHAKRABORTY, K. & MUKHOPADHYAY, A. 2019. Dietary restriction improves proteostasis and increases life span through endoplasmic reticulum hormesis. *Proc Natl Acad Sci U S A,* 116, 17383-17392.
MEISEL, J. D., PANDA, O., MAHANTI, P., SCHROEDER, F. C. & KIM, D. H. 2014. Chemosensation of bacterial secondary metabolites modulates neuroendocrine signaling and behavior of C. elegans. *Cell,* 159, 267-80.
MENEZ, C., ALBERICH, M., COURTOT, E., GUEGNARD, F., BLANCHARD, A., AGUILANIU, H. & LESPINE, A. 2019. The transcription factor NHR-8: A new target to increase ivermectin efficacy in nematodes. *PLoS Pathog,* 15, e1007598.
MENEZ, C., ALBERICH, M., KANSOH, D., BLANCHARD, A. & LESPINE, A. 2016. Acquired Tolerance to Ivermectin and Moxidectin after Drug Selection Pressure in the Nematode Caenorhabditis elegans. *Antimicrob Agents Chemother,* 60, 4809-19.
PAGE, A. P. 2018. The sensory amphidial structures of Caenorhabditis elegans are involved in macrocyclic lactone uptake and anthelmintic resistance. *Int J Parasitol,* 48, 1035-1042.
PARODI, A. J. 2000. Role of N-oligosaccharide endoplasmic reticulum processing reactions in glycoprotein folding and degradation. *Biochem J,* 348 Pt 1, 1-13.
PERENS, E. A. & SHAHAM, S. 2005. C. elegans daf-6 encodes a patched-related protein required for lumen formation. *Dev Cell,* 8, 893-906.
RICHARDSON, C. E., KOOISTRA, T. & KIM, D. H. 2010. An essential role for XBP-1 in host protection against immune activation in C. elegans. *Nature,* 463, 1092-5.
RIERA, C. E., TSAOUSIDOU, E., HALLORAN, J., FOLLETT, P., HAHN, O., PEREIRA, M. M. A., RUUD, L. E., ALBER, J., THARP, K., ANDERSON, C. M., BRONNEKE, H., HAMPEL, B., FILHO, C. D. M., STAHL, A., BRUNING, J. C. & DILLIN, A. 2017. The Sense of Smell Impacts Metabolic Health and Obesity. *Cell Metab,* 26, 198-211 e5.
SANGSTER, N. C. 1994. P-glycoproteins in nematodes. *Parasitol Today,* 10, 319-22.
SHEN, X., ELLIS, R. E., LEE, K., LIU, C. Y., YANG, K., SOLOMON, A., YOSHIDA, H., MORIMOTO, R., KURNIT, D. M., MORI, K. & KAUFMAN, R. J. 2001. Complementary signaling pathways regulate the unfolded protein response and are required for C. elegans development. *Cell,* 107, 893-903.

586 SHEPS, J. A., RALPH, S., ZHAO, Z., BAILLIE, D. L. & LING, V. 2004. The ABC transporter
587 gene family of Caenorhabditis elegans has implications for the evolutionary dynamics
588 of multidrug resistance in eukaryotes. *Genome Biol,* 5**,** R15.
589 TAKATSUKI, A., ARIMA, K. & TAMURA, G. 1971. Tunicamycin, a new antibiotic. I. Isolation
590 and characterization of tunicamycin. *J Antibiot (Tokyo),* 24**,** 215-23.
591 TAYLOR, R. C. & DILLIN, A. 2013. XBP-1 is a cell-nonautonomous regulator of stress
592 resistance and longevity. *Cell,* 153**,** 1435-47.
593

594 **Figure Legends**

595 **Figure 1. Dye filling defective *C. elegans* mutants are resistant to tunicamycin**
596 **A.** Red fluorescence and differential interference contract confocal microscopy images
597 of WT and *osm-3(dh441)IV C. elegans* after DiI treatment.
598 **B.** Developmental tunicamycin (TM) resistance assay using the indicated
599 concentrations with WT animals and *osm-3(dh441)IV* mutants.
600 **C.** Demographic lifespan analysis of WT and *osm-3(dh441)IV* animals. WT mean
601 lifespan = 24 days, *osm-3(dh441)IV* mean lifespan = 29 days, $p<0.0001$.
602 **D.** Developmental TM resistance assay with WT and *daf-10(e1387)V* mutants.
603 **E.** Developmental TM resistance assay with WT and *odr-3(n2150)V* mutants.
604 **F.** Table of dye filling phenotype and TM resistance. In the dye filling column, + is
605 positive for DiI filling as in Figure 1A and - is Dyf. In the TM resistant column, + is
606 resistant and - is not resistant to 10 μg/mL TM.

607 **Figure 1 Supplement 1**
608 **A.** *osm-3(dh441)IV* has a C to T mutation at position 3796925 of exon 8.
609 **B – J.** Developmental TM resistance assay with WT, *odr-1(n1936)X*, *tax-4(p678)III*,
610 *che-11(e1810)V*, *daf-10(e1387)V*, *osm-1(p808)X, osm-6(p811)V, dyf-1(mn335)I*, *che-*
611 *2(e1033)X* and *osm-5(p813)X* mutants.

612 **Figure 2. Tunicamycin-induced ER stress response is blunted in *osm-3* mutants**
613 **A.** DAVID gene ontology (GO) terms that are enriched in TM-treated WT compared to
614 TM-treated *osm-3(dh441)IV* worms. Red = upregulated and blue = downregulated.
615 **B.** Green fluorescent images of WT and *osm-3(dh441)IV* animals in the *hsp-4*::GFP
616 reporter background after 6 hours of 10 μg/mL TM treatment. Worms are outlined in
617 the images.
618 **C.** Biosorter analysis of *osm-3(dh441)IV* vs. WT animals in the *hsp-4*::GFP background
619 after 6 hours of control or TM treatment. Data are mean +SEM, n=4, *** $p<0.0001$ by
620 two-way ANOVA.
621 **D.** Green fluorescent images of WT and *osm-3(dh441)IV* animals in the *hsp-4*::GFP
622 background after development on control or *sel-1* RNAi. Worms are outlined in the
623 images.
624 **E.** Biosorter analysis of *osm-3(dh441)IV* vs. WT animals in the *hsp-4*::GFP background
625 raised on control or *sel-1* RNAi. Data are mean +SEM, n=3, ** $p<0.005$ *** $p<0.0001$
626 by two-way ANOVA.
627 **F.** Quantitative PCR measuring relative *hsp-4* and spliced and unspliced *xbp-1* mRNA
628 levels in WT and *osm-3(dh441)IV animals* after 2 hours of 10 mM DTT treatment. Data
629 are mean +SEM, n=3, * $p<0.05$, ** $p<0.001$, *** $p<0.0001$ by two-way ANOVA.

630 **Figure 2 Supplement 1**
631 **A.** Quantitative PCR measuring relative mRNA expression of indicated genes in WT
632 animals and *osm-3(dh441)IV* mutants after 6 hours of vehicle or TM treatment.

633 **Figure 3. Tunicamycin resistance in *osm-3* mutants is not *daf-16* or *pmk-1***
634 **dependent**
635 **A.** Demographic lifespan analysis of WT, *osm-3(dhh441)IV*, *daf-16(mu86)I* and *osm-*
636 *3(dh441)IV; daf-16(mu86)I* animals. WT mean lifespan = 22 days, *osm-3(dh441)IV*
637 mean lifespan = 25 days $p<0.005$ compared to WT, *daf-16(mu86)I* mean lifespan = 16
638 days $p<0.0001$ compared to WT, *osm-3(dh441)IV*; *daf-16(mu86)I* mean lifespan = 16
639 days $p<0.0001$ compared to WT.
640 **B.** Developmental resistance assay using 10 μg/mL TM with WT, *osm-3(dh441) IV*,
641 *daf-16(mu86) I*, and *osm-3(dh441) IV; daf-16(mu86) I* animals.
642 **C.** Developmental resistance assay using 10 μg/mL TM with WT, *osm-3(dh441) IV* and
643 *daf-2(e1370) III* animals.
644 **D.** *Pseudomonas aeruginosa* PA14 survival assay with WT, *osm-3(dh441) IV*, *pmk-*
645 *1(km25) IV*, and *osm-3(dh441) IV; pmk-1(km25) IV* animals. WT mean survival = 44
646 hours, *osm-3(dh441) IV* mean survival = 58 hours $p<0.001$ compared to WT, *pmk-*
647 *1(km25) IV* mean survival = 31 hours $p<0.001$ compared to WT, *osm-*
648 *3(dh441) IV; pmk-1(km25) IV* mean survival = 34 hours $p<0.001$ compared to WT and
649 $p=0.06$ compared to *pmk-1(km25) IV*.
650 **E.** Developmental resistance assay using 10 μg/mL TM with WT, *osm-3(dh441)IV*,
651 *pmk-1(km25)IV*, and *osm-3(dh441)IV; pmk-1(km25)IV* animals.

652 **Figure 3 Supplement 1**
653 **A.** Biosorter analysis of *osm-3(dh441)IV* vs. WT animals in the *hsp-4*::GFP background
654 raised on control or *daf-16* RNAi. Data are mean +SEM, n=4, *** $p<0.0001$ by two-way
655 ANOVA.

656 **Figure 4. P-glycoprotein inhibition suppresses *osm-3* tunicamycin resistance**
657 **A.** Developmental TM resistance assay using the PGP inhibitor verapamil (VPL) using
658 10 μg/mL TM supplemented with vehicle or 1 nM VPL. Data are mean +SD, n=3, *** p
659 < 0.001 by two-way ANOVA.
660 **B.** Developmental paraquat resistance assay of WT animals and *osm-3(dh441)IV*
661 mutants using 0.2 mM paraquat and vehicle control. Data are mean +SD, n=3, *** p <
662 0.001 by two-way ANOVA.
663 **C.** Developmental ivermectin resistance assay of WT and *osm-3(dh441)IV* mutants
664 using 6 ng/mL ivermectin and vehicle control. Data are mean +SD, n=3, *** p < 0.001
665 by two-way ANOVA.
666 **D.** Demographic lifespan analysis on vehicle and VPL treated WT and *osm-3(dh441)IV*
667 worms. Vehicle treated: WT mean lifespan = 19 days; *osm-3(dh441)IV* mean lifespan
668 = 24 days p<0.0001 compared to WT vehicle. VPL treated: WT mean lifespan = 19
669 days; *osm-3(dh441)IV* mean lifespan = 22 days, p<0.005 compared to WT Vehicle.

670 **Figure 4 Supplement 1**
671 **A.** Heat shock assay at 35°C in WT and *osm-3(dh441)IV* animals on day 1 of
672 adulthood. WT mean survival = 7 hours, *osm-3(dh441)IV* mean survival = 6 hours,
673 p<0.01
674 **B.** Hydrogen peroxide survival assay using 1μM H_2O_2 on day 1 of adulthood in WT
675 and *osm-3(dh441)IV* animals. WT mean survival = 7 hours, *osm-3(dh441)IV* mean
676 survival = 6 hours, no significant difference
677 **C.** WT development on 0 to 1μM Verapamil. No significant difference in development.
678

679 **Figure 5. *nhr-8* signaling regulates xenobiotic detoxification response through**
680 **PGPs**
681 **A.** Quantitative PCR measuring relative PGP mRNA expression in WT, *osm-*
682 *3(dh441)IV*, *nhr-8(hd117)IV* and *osm-3(dh441)IV; nhr-8(hd117)IV* animals. Data are
683 mean +SEM, n=3, * p<0.05, ** p<0.001, *** p<0.0001 by two-way ANOVA.
684 **B.** Developmental TM resistance assay on 10 μg/mL TM and control with WT, *osm-*
685 *3(dh441)IV*, *nhr-8(hd117)IV* and *osm-3(dh441)IV; nhr-8(hd117)IV* animals. Data are
686 mean +SD, n=3, * p<0.05, *** p<0.0001 by t-test.
687 **C.** Quantitative PCR measuring relative *pgp-8* mRNA expression in WT and *nhr-8*
688 overexpressing (*nhr-8* OE) extrachromosomal array dhEx451[*coel::rfp;nhr-8::gfp*].
689 Data are mean +SEM, n=3, * p<0.05 by t-test.
690 **D.** Developmental dose response TM resistance assay using the indicated TM
691 concentrations with transgenic animals containing an *nhr-8* overexpressing
692 extrachromosomal array dhEx451[*coel::rfp;nhr-8::gfp*]. "- Ex Array" do not visibly
693 contain the extrachromosomal array as judged by the co-injection marker and "+ Ex
694 Array" contain the extrachromosomal array. Data are mean +SEM, n=3, * p<0.05 and
695 *** p<0.005 by two-way ANOVA. At least 100 animals were used in each condition.
696 Transmission rates of the extrachromosomal array was assayed on parallel plates.
697 **E.** Biosorter analysis of *osm-3(dh441)IV* in the *hsp-4*::GFP background raised on
698 control or *pgp-8* RNAi after 6 hours of control or 20 μg/mL TM treatment. Data are
699 mean +SEM, n=3, * p<0.05, *** p<0.0001 by two-way ANOVA.

700 **Figure 5 Supplement 1**
701 **A.** Demographic lifespan analysis of WT, *osm-3(dh441)IV, nhr-8(hd117)IV and osm-*
702 *3(dh441)IV;nhr-8(hd117)IV* animals. WT mean lifespan = 22 days, *osm-3(dh441)IV*
703 mean lifespan = 24 days p<0.0001 compared to WT, *nhr-8(hd117)IV* mean lifespan =
704 *14* p<0.0001 compared to WT*, osm-3(dh441)IV;nhr-8(hd117)IV* mean lifespan = 19
705 days p<0.0001 compared to WT.

706 **Figure 6. Sterol signals modulate TM resistance**
707 **A.** Developmental dose response TM resistance assay using the indicated TM
708 concentrations with WT animals and *osm-3(dh441)IV* mutants raised on 0 or 5 μg/mL
709 cholesterol.
710 **B.** Cholesterol dose response developmental assay with WT, *osm-3(dh441)IV*, *nhr-*
711 *8(hd117)IV* and *osm-3(dh441)IV; nhr-8(hd117)IV* animals on vehicle or 5 μg/mL TM.
712 **C.** Biosorter analysis of WT animals with the *hsp-4*::GFP reporter raised on 0 or 50
713 μg/mL cholesterol after 6 hours of vehicle or 5 μg/mL TM treatment. Data are mean
714 +SEM, n=3, * p<0.05, *** p<0.0001 by two-way ANOVA.
715 **D.** Quantitative PCR measuring relative *pgp-8* mRNA expression in WT animals raised
716 on 0 or 5 μg/mL cholesterol. Data are mean +SEM, n=3, * p<0.05 by t-test.

Figure 1. Dye filling defective *C. elegans* mutants are resistant to tunicamycin

A.

B.

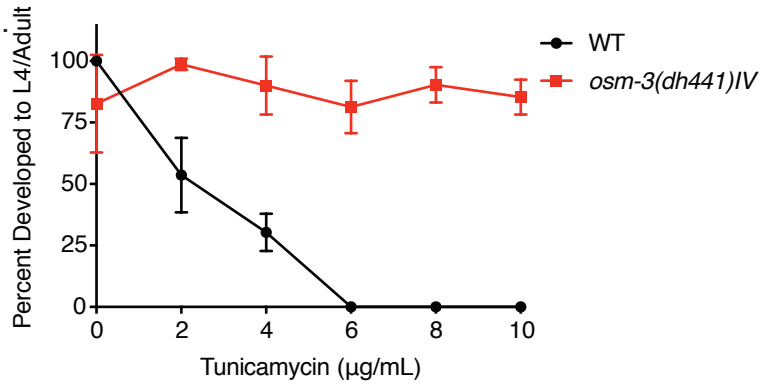

C.

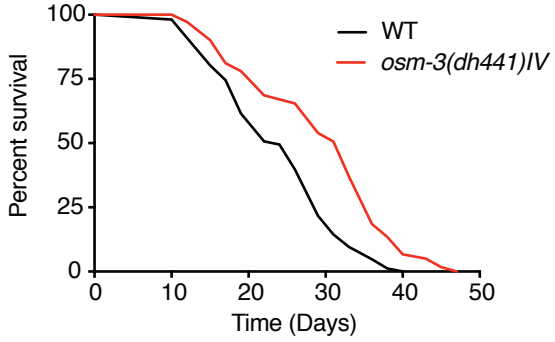

D.

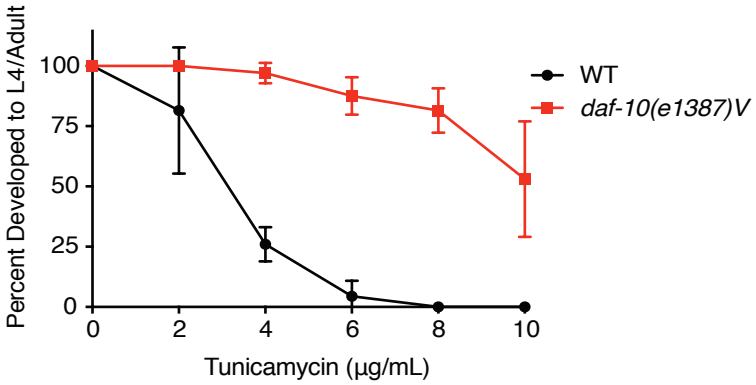

E.

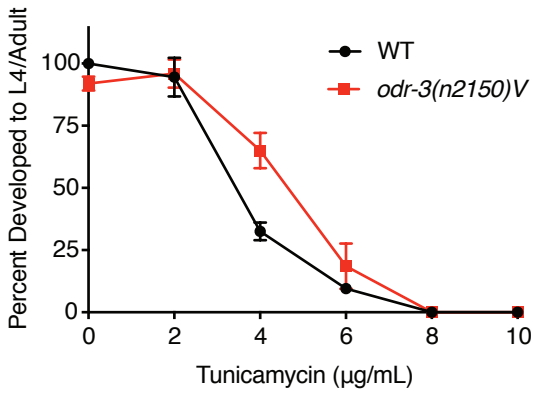

F.

	Dye Filling	Tunicamycin Resistant
Wild type	+	-
odr-1(n1936)X	+	-
odr-3(n2150)V	+	-
tax-4(p678)III	+	-
che-2(e1033)X	-	+
che-11(e1810)V	-	+
daf-6(e1377)X	-	+
daf-10(e1387)V	-	+
dyf-1(mn335)I	-	+
osm-1(p808)X	-	+
osm-3(dh441)IV	-	+
osm-5(p813)X	-	+
osm-6(p811)V	-	+

Figure 2. Tunicamycin induced ER stress response is blunted in osm-3

TM treated Wild type vs. *osm-3(dh441)IV*

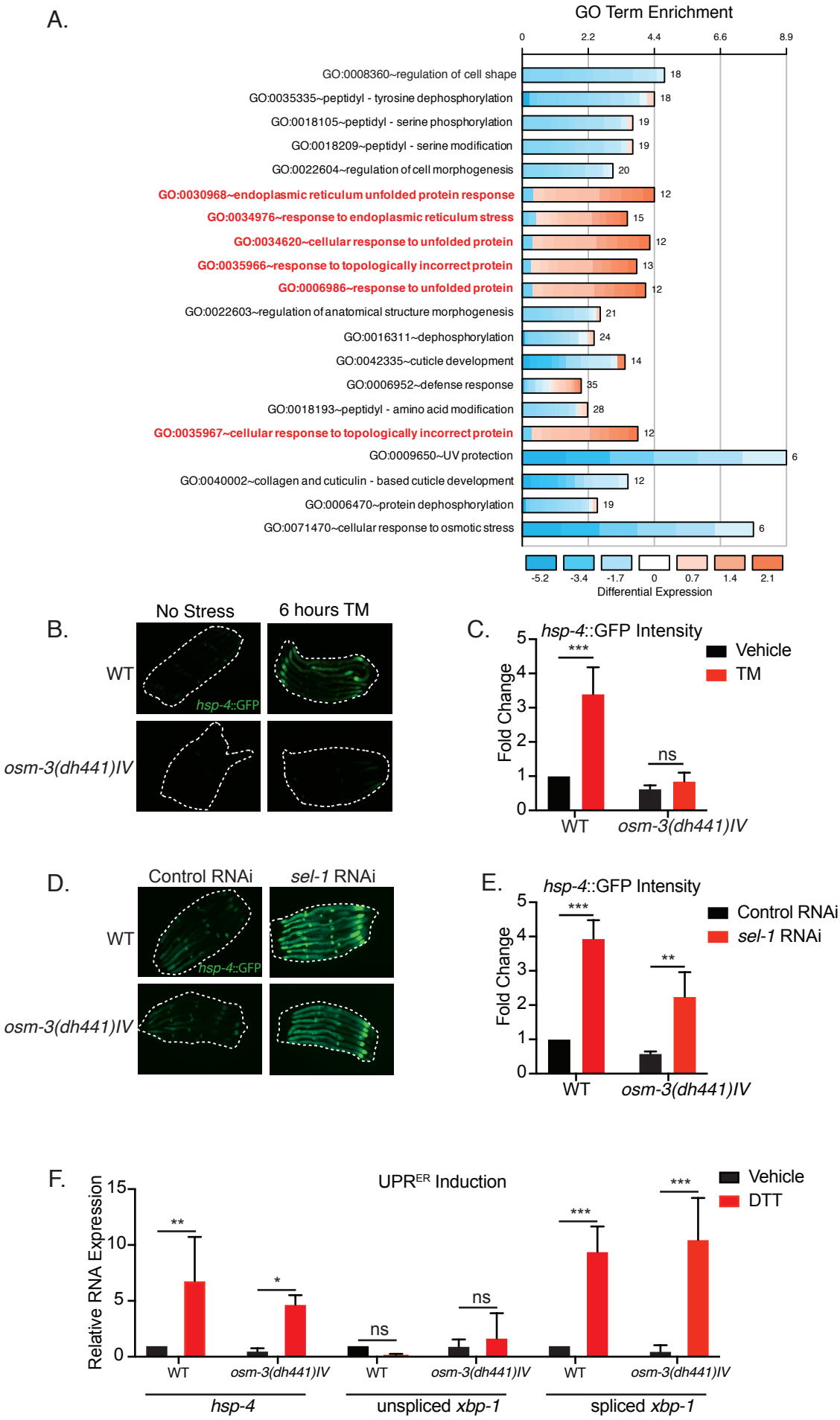

Figure 3. Tunicamycin resistance in *osm-3* is not *daf-16*/IIS or *pmk-1* dependent

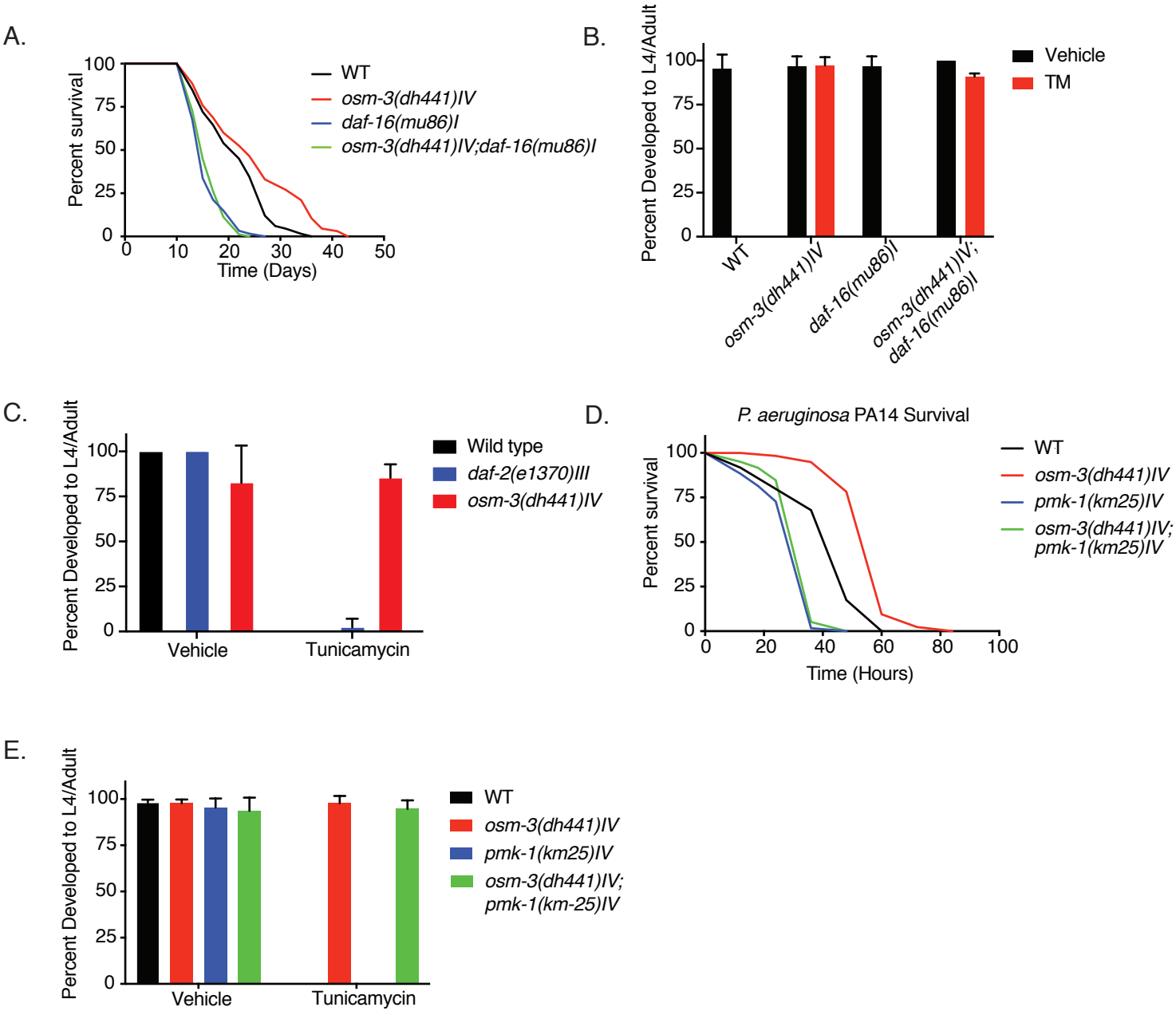

Figure 4. P-glycoprotein inhibition supresses *osm-3* TM resistance

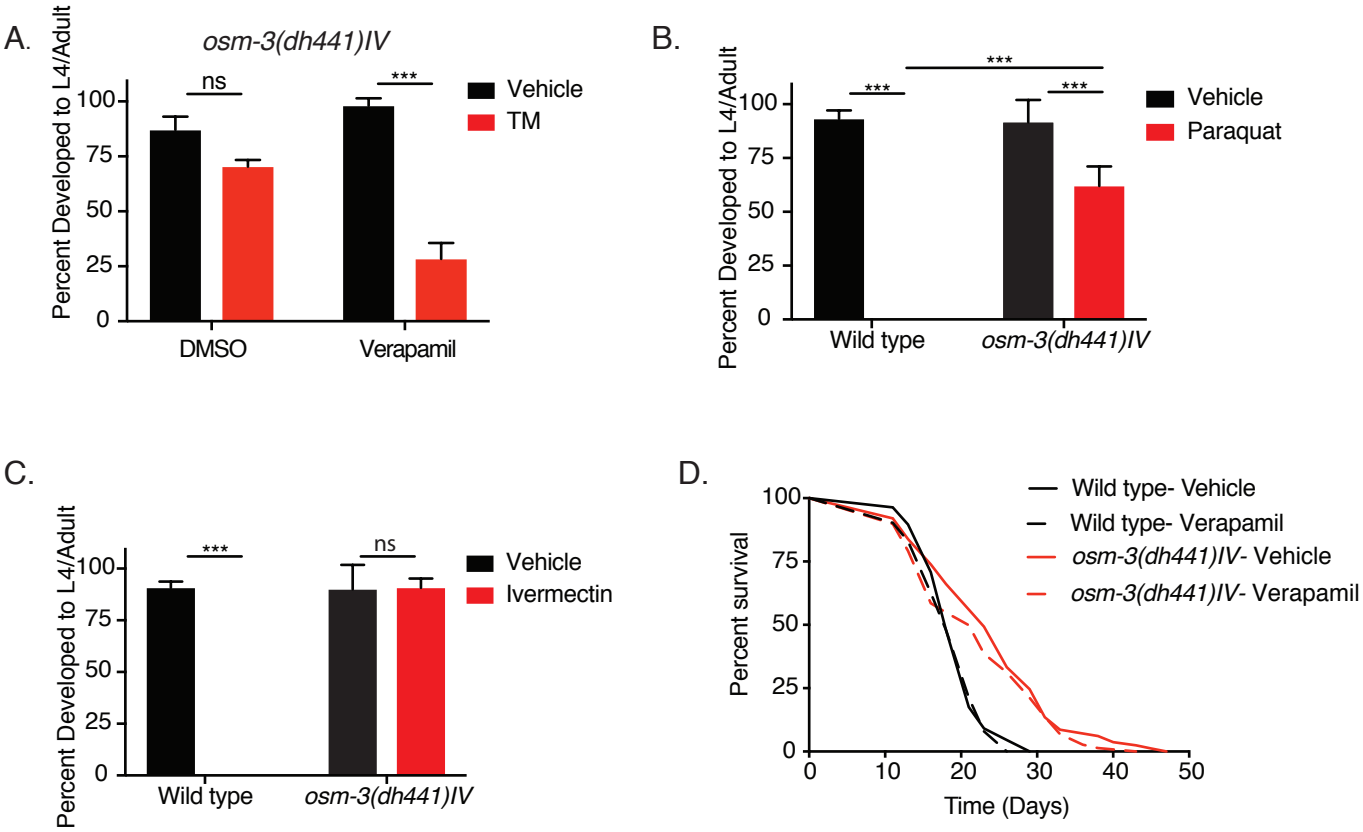

Figure 5. *nhr-8* signaling regulates xenobiotic detoxification response through PGPs

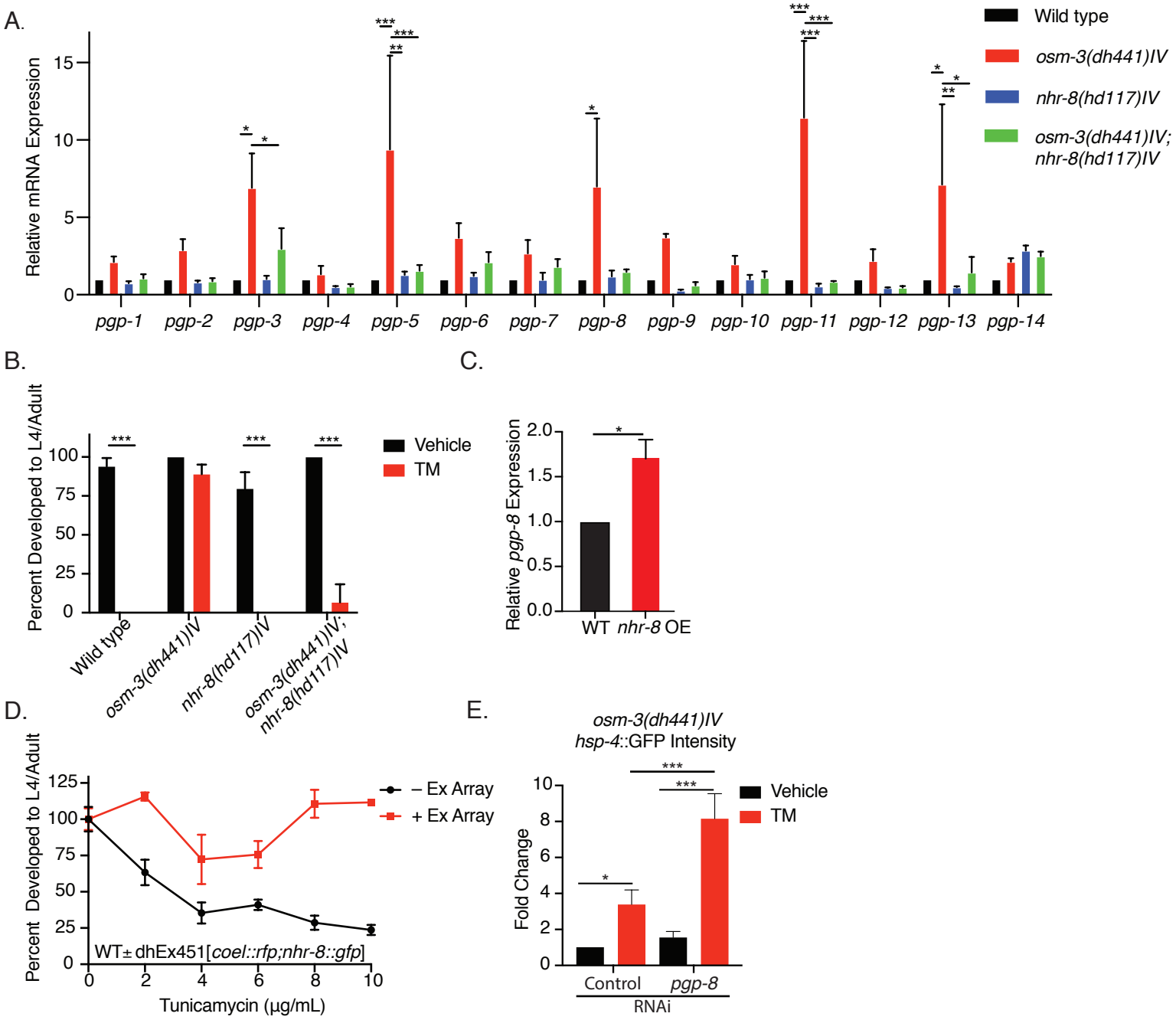

Figure 6. Sterol signals modulate TM resistance

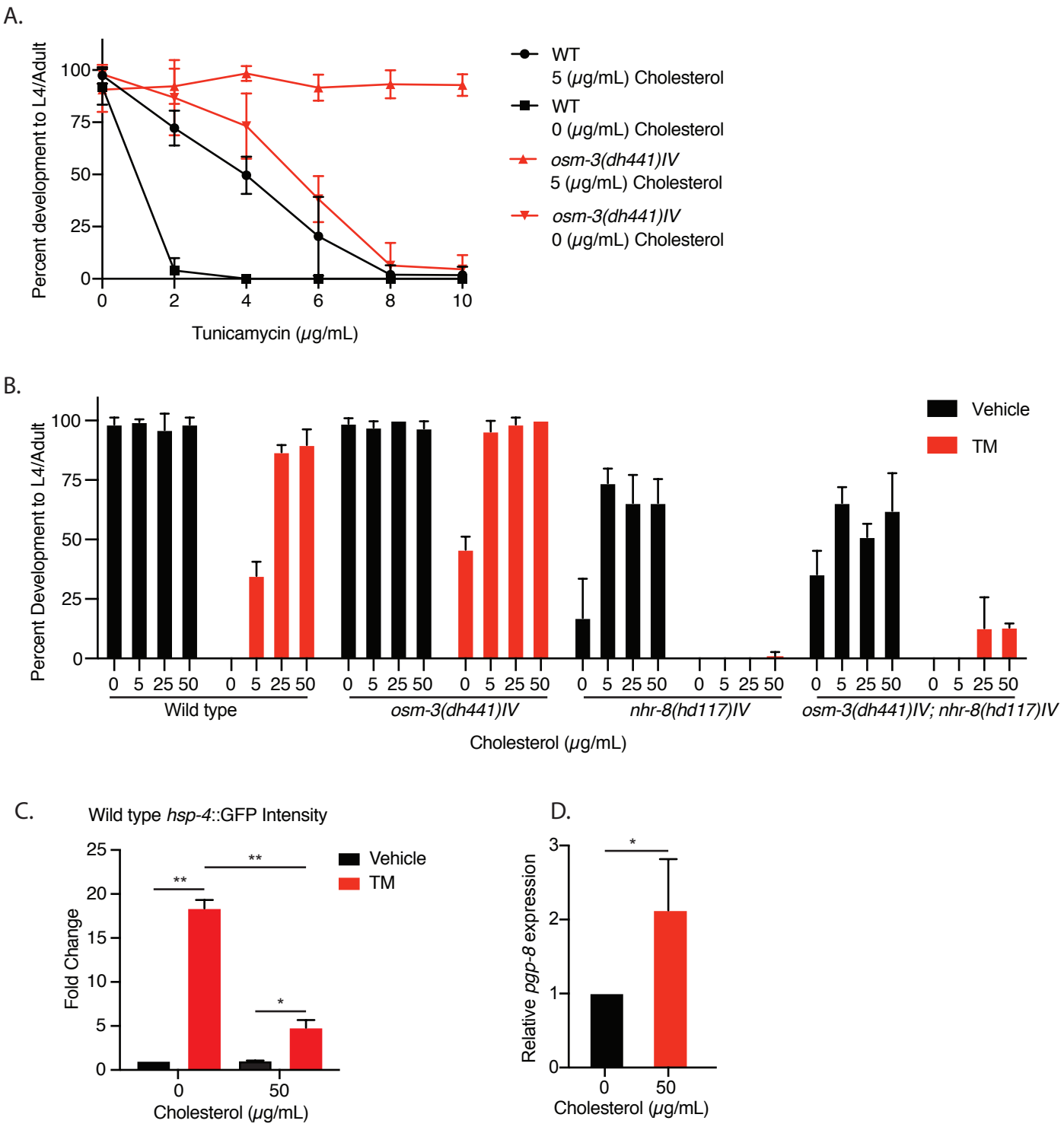

Supplementary Figure 1.

A.

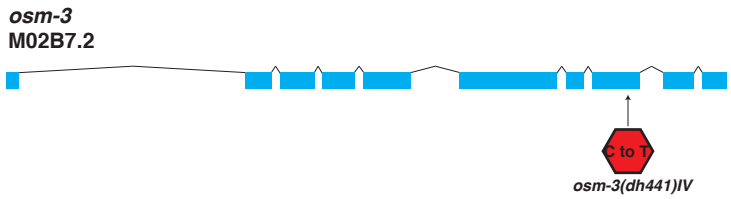

B.

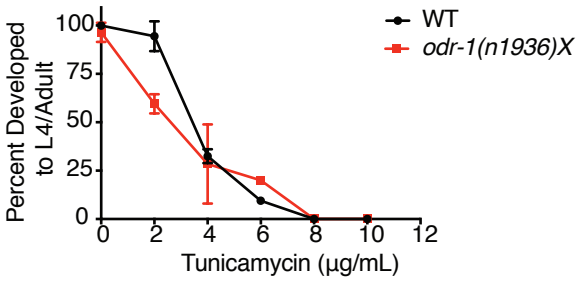

C.

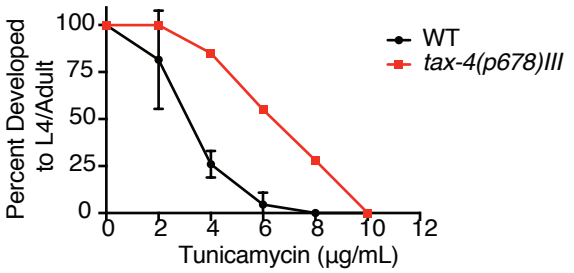

D.

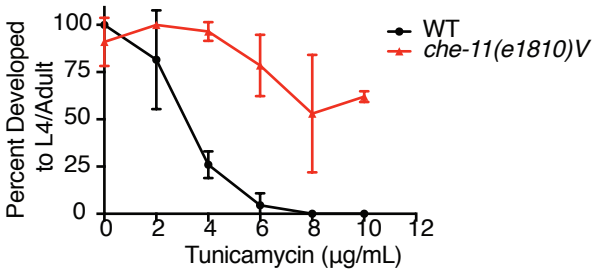

E.

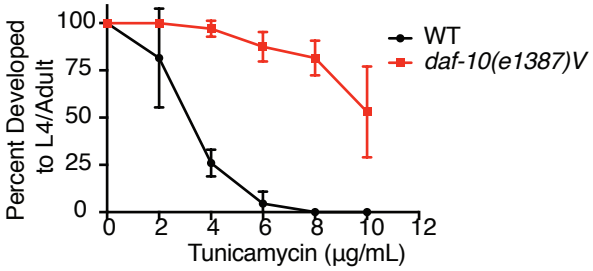

F.

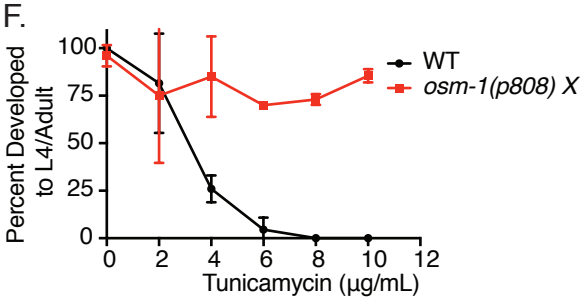

G.

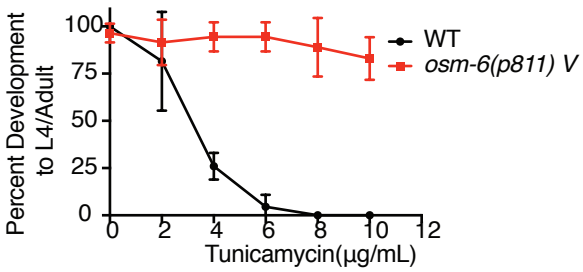

H.

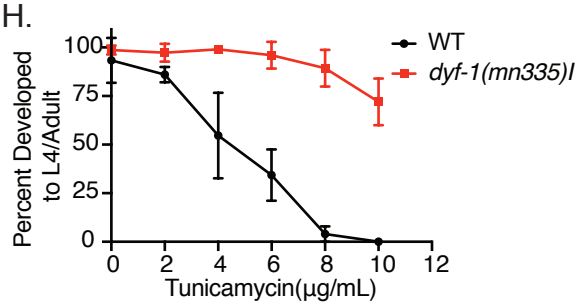

I.

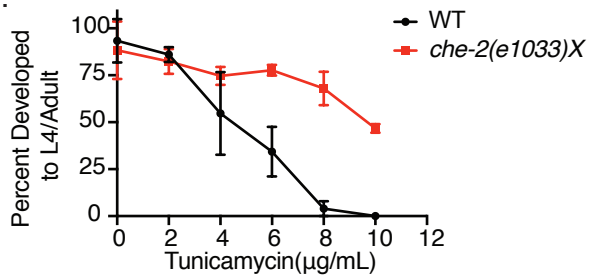

J.

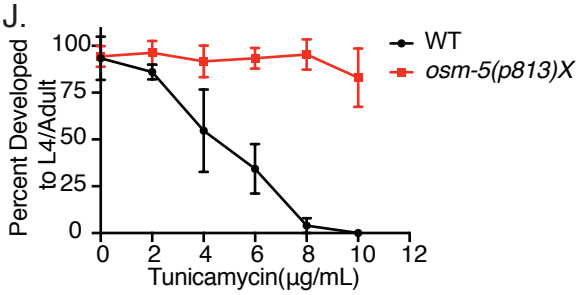

Supplementary Figure 2.

A.

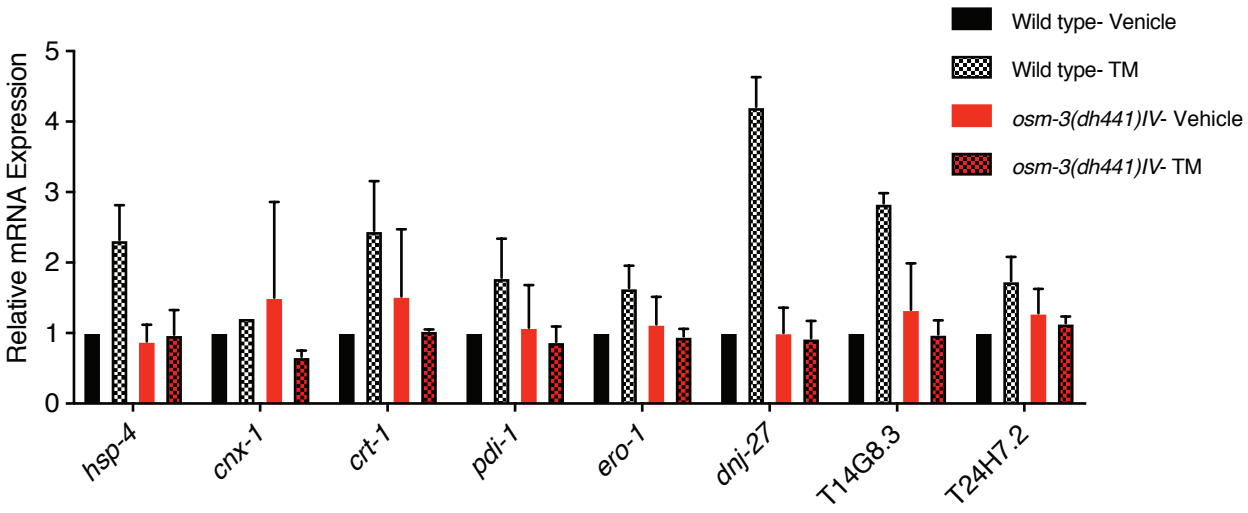

Supplementary Figure 3.

A.

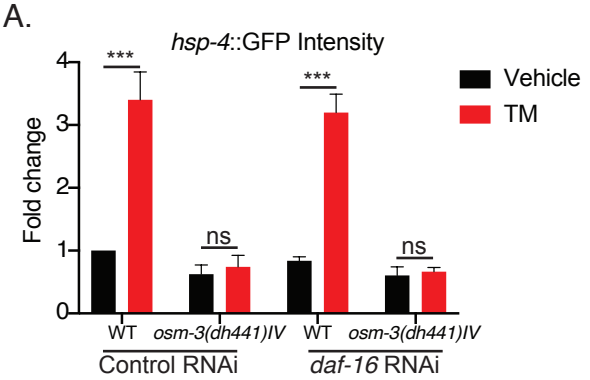

Supplementary Figure 4.

A.

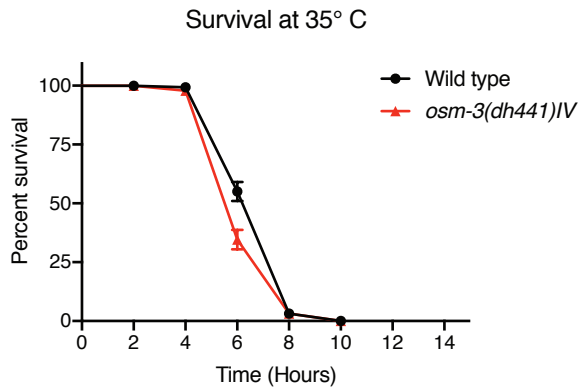

B.

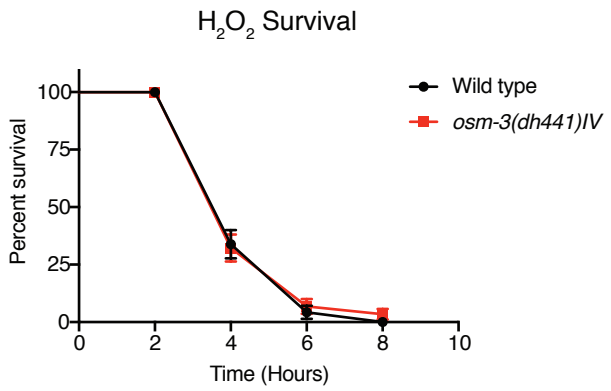

C.

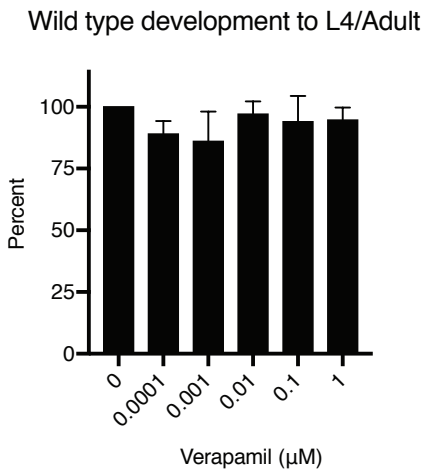

Supplementary Figure 5.
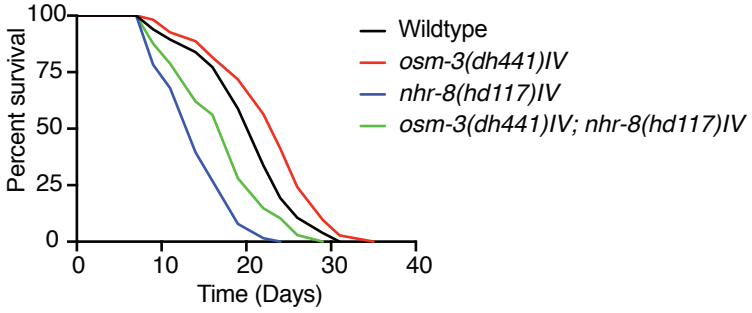
A.